ARTICLE

Interface Engineering Strategies towards $Cs_2AgBiBr_6$ Single-Crystalline Photodetectors with Good Ohmic Contact Behaviours

Received 00th January 20xx,
Accepted 00th January 20xx

DOI: 10.1039/x0xx00000x

Yangyang Dang, Guoqing Tong, Wentao Song, Zonghao Liu, Longbin Qiu, Luis K. Ono and Yabing Qi*

Lead-free double perovskite materials have attracted much interest in the optoelectronic applications due to their nontoxicity and high stability. In this work, centimetre-sized $Cs_2AgBiBr_6$ single crystals were successfully grown using methylammonium bromide (MABr) as the flux by top-seeded solution growth (TSSG) method. The low-temperature crystal structure of $Cs_2AgBiBr_6$ single crystals was determined and refined. To investigate the interface problems between $Cs_2AgBiBr_6$ single crystal and electrodes, the optical band gap, X-ray photoelectron spectroscopy (XPS), and ultraviolet photoemission spectroscopy (UPS) measurements were performed on $Cs_2AgBiBr_6$ single crystals. More importantly, we investigated the photodetectors based on $Cs_2AgBiBr_6$ single crystals with different contact electrodes (Au, Ag, and Al). It is found that a good Ohmic contact with Ag electrodes enables excellent photo-response behaviors. Furthermore, we studied the photodetectors based on $Cs_2AgBiBr_6$ 6 single crystals using Ag electrodes under room and low temperature conditions, which underwent phase transition. $Cs_2AgBiBr_6$ single crystal photodetectors show clear differences at room and low temperatures, which is caused by the work function changes of $Cs_2AgBiBr_6$ single crystals induced by the reversible phase transition. These attractive properties may enable the opportunities to apply emerging double perovskite single-crystalline materials for high-performance optoelectronic devices.

Introduction

Lead (Pb)-based hybrid perovskite materials have attracted tremendous attention owing to their outstanding properties when applied in photovoltaic devices.[1-2] Power conversion efficiencies (PCEs) as high as 25.2 % have been achieved for Pb-based perovskite solar cells.[3] However, the toxicity and instability of Pb-based perovskite materials need to be solved. It is imperative to search for alternative perovskite materials containing only non-toxic elements. A strategy is to replace the toxic Pb^{2+} with two different oxidation states Ag^{+} and Bi^{3+} to form the double perovskite materials.[4] Several nontoxic candidates such as Cs_2AgBiX_6 (X = Cl, Br),[5] $(CH_3NH_3)_2AgBiBr_6$[6] and so on, have been reported. Especially, $Cs_2AgBiBr_6$ is considered to be an appealing lead-free semiconducting material due to its promising optoelectronic properties.[7] Woodward and coworkers reported the solid-state synthesis, and the crystal structure of Cs_2AgBiX_6 (X=Cl, Br) with the cubic system with *F*m-3m (no.225) by the powder X-ray diffraction (PXRD) experiments and Rietveld refinements.[5] The computational design and the experimental synthesis of Pb-free halide double perovskites including the band gaps and stability of Cs_2AgBiX_6 (X=Cl, Br) were reported by Giustino et al.[8-10] Band structure calculations of $Cs_2AgBiBr_6$ perovskite based on the order-disorder transition by first principle study were performed in detail by Wei et al.[11] Structural analysis and optical properties of $Cs_2AgBiBr_6$ powder samples below and above the phase transition point were introduced by Schade et al. The authors reported the low-temperature and room-temperature crystal structure parameters on the basis of neutron powder diffraction (NPD), but did not obtain the single-crystal structure.[12] Zhan and coworkers investigated the application of $Cs_2AgBiBr_6$ thin films as humidity sensors, which exhibited superfast recovery times as well as high stability.[13] In many cases, optoelectronic devices, such as solar cells[14-15] and X-ray detectors [16] based on double perovskites are in the form of pressed powder (pellets) and thin films.

Single crystals with absence of grain boundaries and low densities of traps provide an ideal test platform for fundamental studies on the properties of double perovskites. For example, in a study employing a single crystal $CH_3NH_3PbI_3$ perovskite sample (thickness = 20 μm), an outstanding PCE of 21.09% and fill factor (FF) up to 84.3% were reported.[17] Therefore, it will be interesting to employ $Cs_2AgBiBr_6$ double perovskite single crystals in the optoelectronic applications, but currently such studies are still scarce. In 2016, Karunadasa and coworkers reported for the first time the room-temperature crystal structure and fundamental optical properties of $Cs_2AgBiBr_6$ single crystals obtained by the temperature-cooling method.[18] Tang and coworkers reported the X-ray detectors based on $Cs_2AgBiBr_6$ single crystals, which exhibited a low detection limit.[19] Roeffaers and coworkers studied the photophysical properties of $Cs_2AgBiBr_6$ single-crystalline X-ray detectors influenced by the carrier dynamics at both room- and liquid nitrogen-temperatures.[20] Recently, Gao and coworkers have studied the reversible thermochromism and device fabrications of $Cs_2AgBiBr_6$ based on

Energy Materials and Surface Sciences Unit (EMSSU), Okinawa Institute of Science and Technology Graduate University (OIST), 1919-1 Tancha, Onna-son, Kunigami-gun, Okinawa 904-0495, Japan
Email: Yabing.Qi@OIST.jp
Electronic Supplementary Information (ESI) available: [Crystal structure, XPS, SCLC, Energy level, and photo-response based on Au and Al electrodes]. See DOI: 10.1039/x0xx00000x

both single crystals and thin films.[21] Meanwhile, Fan et al. observed the regulation of the order-disorder phase transformations in $Cs_2AgBiBr_6$ single crystal in an X-ray detector by the addition of the phenylethylamine bromide (PEABr), which exhibited obvious ordered arrangements.[22] In these studies, however, hysteresis phenomena in the I-V curves were evident in $Cs_2AgBiBr_6$ single crystal X-ray detectors based on gold (Au) electrodes.[19-20, 22] Zhang et al. reported the optical and electrical properties of $Cs_2AgBiBr_6$ double perovskite single crystals.[23]Until now, there have been no reports about the interfaces between $Cs_2AgBiBr_6$ single crystal and electrodes in their photodetectors.

In this work, centimeter-sized $Cs_2AgBiBr_6$ single crystals were successfully grown using MABr as the flux in the mother solution by TSSG method. The crystal structure of $Cs_2AgBiBr_6$ single crystals below the phase transition point was systematically studied. To investigate the interface relationships between $Cs_2AgBiBr_6$ single crystal and electrodes as well as the band gap, XPS and UPS measurements were performed on $Cs_2AgBiBr_6$ single crystals. More importantly, we investigated the photodetectors based on $Cs_2AgBiBr_6$ single crystals with different electrodes of gold (Au), silver (Ag), and aluminum (Al) at different wavelengths under both ambient air (relative humidity = 20 %) and vacuum. It is demonstrated that $Cs_2AgBiBr_6$ single crystal-based photodetectors using Ag electrodes exhibit better Ohmic contact behaviors than Au and Al. We also performed a systematic study on $Cs_2AgBiBr_6$ single crystal-based photodetectors using Ag electrodes at room and low temperature, and the other two cases showed clear differences in photo-response and hysteresis. These properties may enable new opportunities to apply these emerging double perovskites single crystalline materials in high performance optoelectronic devices.

Results and discussion

Bulk $Cs_2AgBiBr_6$ single crystals with the dimensions of 10 mm × 9 mm × 6 mm (Fig. 1a) were grown using MABr as the flux in the HBr-H_3PO_2 mixed solution in ambient atmosphere, according to previous crystal growth methods.[24-27] The theoretical morphology deduced by the Bravais-Friedel-Donnay-Harker (BFDH) method [28] are shown in Fig. 1b. The theoretical crystal facets are determined to be (200) and (111) The single crystal growth requires proper solubility, flux, saturation, and temperature control. We used the seed crystal growth method to select the seed crystal direction to control the shape and size. Thus, we could obtain controllable shape and size, which led to good device reproducibility. It is easier to obtain large size $Cs_2AgBiBr_6$ single crystals with MABr as flux as shown in Fig. S1, because MABr can increase the solubility for $Cs_2AgBiBr_6$ single crystal growth owing to the enhanced dissolution of $Cs_2AgBiBr_6$ materials induced by MABr. The growth of $Cs_2AgBiBr_6$ single crystal was performed in saturated perovskite precursor solutions. Meanwhile, the crystal structure of $Cs_2AgBiBr_6$ at room temperature (Fig. 1c and Table S1) was determined and refined with the formula of $Cs_4Ag_2Bi_2Br_{12}$, which exhibits the cubic space group *F*m-3m (no. 225) consistent with the previous report.[18] Based on the previous report about the crystal structure under phase transition from the powder sample, [12] we carried out the low-temperature crystal structure measurements. The crystal structure determinations and refinements at 100 K by single-crystal X-ray diffraction analysis demonstrated that there were two possibilities of the pseudopolymorphic phase, i.e., tetragonal or cubic space groups (Table S1). Based on the previous report,[12] $Cs_2AgBiBr_6$ single crystal undergoes a reversible phase transition (Fig. S2 and Table S1). The related crystal parameters are listed in Table S1 in Supporting Information. It is demonstrated that $Cs_2AgBiBr_6$ single crystal at 100 K exhibits the tetragonal space group I4/m (no. 87), which is consistent with the report by Schade et al.[12] Based on the single crystal determination, we did not observe MA cations in the low temperature crystal structure. Therefore, it is verified that there exists no MABr in $Cs_2AgBiBr_6$ single crystals. Moreover, in Fig. 1d we did not observe redundant peaks about MABr. Besides, the N 1s peak was not observed according to XPS in Fig. S3. PXRD pattern agrees well with the simulated XRD diffraction pattern of $Cs_2AgBiBr_6$ single crystals, as shown in Fig. 1d.

XPS was employed to further determine the elemental composition of $Cs_2AgBiBr_6$ double perovskites.[29-31] Although $Cs_2AgBiBr_6$ single crystals are stable in ambient atmosphere, to avoid the influences of oxygen and humidity on the surface of each single crystal, the surface of each single crystal was first cleaved by a sharp knife in Ar atmosphere and then polished by abrasive paper and silk textile (Fig. 2a, S3a, and S4). The XPS survey in Fig. S3b reveal that these single crystal samples have high percentage atomic concentrations of Cs, Ag, Bi and Br, and the amount of C and O is negligible. The high-resolution XPS spectra of Cs 3d, Ag 3d, Bi 4f, and Br 3d core levels are shown in Fig. S3c-f. The peaks at the binding energies of 724.6 eV and 738.6 eV are attributed to the Cs $3d_{5/2}$ and $3d_{3/2}$ core levels (Fig. S2c), respectively. The peaks located at the binding energies of 368.1 eV and 374.1 eV are attributed to the Ag $3d_{5/2}$ and $3d_{3/2}$ core levels (Fig. S3d), respectively. The peaks located at the binding energies of 159.2 eV and 164.6 eV are attributed to Bi $4f_{7/2}$ and $4f_{5/2}$ core levels (Fig. S3e), respectively. The peaks located at the binding energies of 68.5 eV and 69.5 eV are attributed to the Br $3d_{5/2}$ and $3d_{3/2}$ core levels (Fig. S3f), respectively. These results are consistent with the previous report on $Cs_2AgBiBr_6$ thin films.[29] To determine the detailed electronic structure, we performed UPS measurements on the single crystal samples to determine the work function (WF) and valence band maximum (VBM). The UPS survey based on the $Cs_2AgBiBr_6$ single crystal is shown in Fig. 2c. Based on the secondary electron onset of the UPS spectrum (Fig. 2c), the WF value of $Cs_2AgBiBr_6$ single crystals is determined to be 4.28 eV, which is smaller than that (5.01 eV) of the $Cs_2AgBiBr_6$ thin film samples.[29] Similarly, in previous reports, the WF value of $MAPbBr_3$ single crystals was determined to be 4.61 eV,[32] while the WF value of $MAPbBr_3$ thin films was determined to be 5.12 eV.[33] The ionization energy is defined as the energy difference between the vacuum level and VBM. Kahn and co-workers proposed the determination of VBM onsets in perovskites to be conducted in semi-log plots. [34-35] Accordingly, we obtained the VBM of 5.64 eV. The ionization energy value is determined to be 5.64 eV (Fig. 2c), which is smaller than the previously reported value based on the $Cs_2AgBiBr_6$ thin films (7.13 eV).[29] The results are possibly caused by the following reasons: 1) different preparation methods can have an influence on the perovskite energy levels;[36a] 2) single crystals exhibit no grain boundaries and low densities of traps, while polycrystalline thin films have grain boundaries and high densities of electronic traps.[36b] Combined with the optical band gap (2.0 eV) from Fig. 2b, the

conduction band minimum (CBM) is deduced to be at a position of 3.64 eV below the vacuum level in Fig. 2d. It seems that the WF of $Cs_2AgBiBr_6$ single crystal theoretically matches well with the electrodes in the order of Al > Ag > Au according to their energy levels.

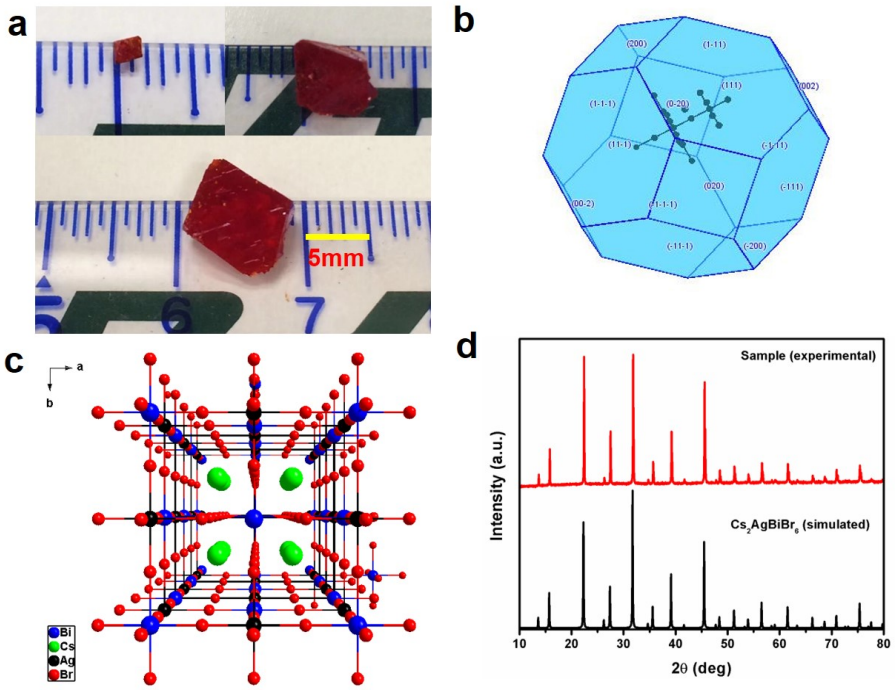

Fig. 1 (**a**) Photos of a $Cs_2AgBiBr_6$ single crystal; (**b**) Theoretical morphology of the $Cs_2AgBiBr_6$ single crystal deduced by the Bravais-Friedel-Donnay-Harker (BFDH) method;[28] (**c**) Crystal structure of $Cs_2AgBiBr_6$ at room temperature; (**d**) Comparison between the experimental and simulated X-ray diffraction patterns for $Cs_2AgBiBr_6$.

The quality of the $Cs_2AgBiBr_6$ single crystals is verified by evaluating the trap state density, mobility and PL decay lifetime (Fig. S5 and Fig. S6). The obtained high-quality $Cs_2AgBiBr_6$ single crystals were cleaved and polished by mechanical processing (Fig. S4) before incorporating into Au/ $Cs_2AgBiBr_6$ thin single crystal/Au vertical device as shown in Fig. S5. The trap state density (n_{trap}) in the $Cs_2AgBiBr_6$ single crystal was determined by the dark current-voltage (I-V) measurement and analyzing the trap filling limit voltage (V_{TFL}), as shown in Fig. S5a. It is found that there exist three regions in the dark J-V curve. With the increase of the applied voltage V, the current (I) increases linearly, which shows the Ohmic behavior (n=1) between the Au electrode and the perovskite when the applied voltage is low than the first inflection point voltage [35]. Further increase in applied voltage leads to a fast-nonlinear rise (n>3) in the current. The first inflection point voltage is associated with the trap filling process, and the trap state density and carrier mobility can be computed according to Equation 1 and Equation 2[37]

$$V_{TFL} = \frac{en_{trap}d^2}{2\varepsilon_0\varepsilon} \qquad (1)$$

$$\mu = \frac{8}{9}((J_d L^3)/(\varepsilon\varepsilon_o V^2)) \qquad (2)$$

where d is the thickness of the $Cs_2AgBiBr_6$ single crystal in Fig. S5b, ε is the relative dielectric constant for $Cs_2AgBiBr_6$ (ε =51),[19] and ε_0 is the vacuum permittivity. However, Steele et al. reported the trap density by using the dielectric constant $\varepsilon = 5.8$. Therefore, our result based on the extracted trap density from V_{TFL} is one order larger than the previous report.[20] ε_0 is the vacuum permittivity. The trap state density n_{trap} and carrier mobility μ is calculated using Equations (1) and (2). The V_{TFL} for $Cs_2AgBiBr_6$ is 3.48 V, as shown in Fig. S5a and the corresponding trap state density is 3.58 × 10^{10} cm^{-3}. The carrier mobility μ is 0.49 cm^2 V^{-1} s^{-1}. Besides, the average carrier lifetime of $Cs_2AgBiBr_6$ single crystals is 2.39 ns according to the biexponential fitted formula (Fig. S6), which is shorter than thin films and powders.[45] The measured low trap state density and verifies the high quality of our $Cs_2AgBiBr_6$ single crystals.

To obtain high-performance optoelectronic devices, it is important to clarify the impact of the interface between $Cs_2AgBiBr_6$ single crystals and electrodes. Insertion of interface layers between perovskite crystals and top electrodes has been demonstrated to attain Ohmic contacts by proper energy.[15, 17] For example, Wu *et al.* employed P3HT between the perovskite crystal $Cs_2AgBiBr_6$ and the Au electrode.[15] On the other hand, the search for a viable electrode leading to a good Ohmic contact in $Cs_2AgBiBr_6$ single-crystal photodetectors is also advantageous considering the simplicity of the device structure. We first investigate the crystal/electrode interface of the $Cs_2AgBiBr_6$ single crystal photodetectors equipped with different electrodes under illumination at different wavelengths at room temperature in air and vacuum atmosphere. Fig. 3 and Fig. S7 illustrate the photodetectors based on the $Cs_2AgBiBr_6$ single crystals coated with different electrodes (Au, Ag, and Al), with an electrode area of 1 mm^2 in length and width, channel = 50 μm, and thickness ≈ 80 nm. For photodetector measurements, solar simulator is used as light source and the power density is close to 66.3 mW cm^{-2}. The

influences of oxygen and humidity on $Cs_2AgBiBr_6$ single crystalline photodetectors were investigated employing a probe station that allows vacuum pumping and controlled atmosphere. We investigated the differences in photo-responses of $Cs_2AgBiBr_6$ single crystal photodetectors with different electrodes in air and under vacuum conditions. Fig. 3 and Fig. S7 show the I-V curves and photo-responses in air with the light turned on and off for several cycles. In addition, the photodetectors based on Au and Al electrodes under vacuum exhibited current hysteresis phenomena, which is consistent with previous reports based on Au electrodes.[19-20, 22] It is concluded that oxygen and H_2O may reduce current hysteresis phenomena. The work function of the $Cs_2AgBiBr_6$ single crystal theoretically matches well Al electrodes (Fig. 2d). However, Al tends to react with the $Cs_2AgBiBr_6$ single crystal, which leads to poor photodetector performance and hysteresis phenomenon. Similarly, Ahmad and co-workers investigated the interfacial properties of Al and Ag contacts on $MAPbBr_3$ single crystals, and they also found that Al easily reacted with $MAPbBr_3$ perovskite crystals.[38] Interestingly, $Cs_2AgBiBr_6$ single crystal-based photodetectors using Ag electrodes exhibited excellent photo-response behaviours both in air and vacuum. In Table S2, the calculated responsivity of $Cs_2AgBiBr_6$ single crystal devices in air and vacuum at 293 K is 0.9 and 0.92 mAW^{-1} for the device under 400 nm illumination with a bias of 5 V, respectively. In addition, we assume that the dark current is dominated by the shot noise for estimating D* (Supporting Information, Equation (2)).[46c] The corresponding detectivity (D*) of the device is calculated to be 1.38×10^9 and 2.66×10^9 Jones (Jones = cm $Hz^{1/2}$ W^{-1}), respectively.[46] The ON/OFF ratio of the devices in air and vacuum at 293 K is 42 and 153 at a bias of 5 V, respectively, which exhibits better performance than thin film-based photodetectors previously reported by He and co-workers. [29] Compared with Au and Al electrodes (Fig. S7d, h), $Cs_2AgBiBr_6$ single crystal photodetectors using Ag electrode exhibit stable photo-response in vacuum at 293 K (Fig. 3b, d). This observation is attributed to the excellent Ohmic contact of Ag with the $Cs_2AgBiBr_6$ single crystal.

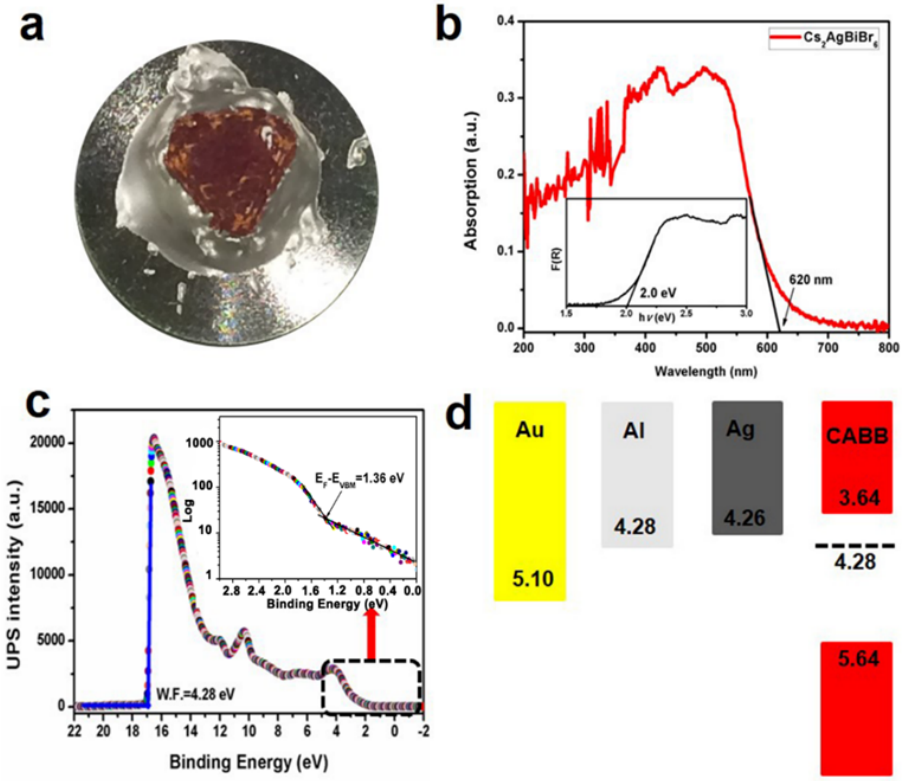

Fig. 2 (a) The photo of Cs2AgBiBr6 single crystal measured by XPS and UPS; (b) Optical band gap of $Cs_2AgBiBr_6$ material; (c) UPS of $Cs_2AgBiBr_6$ single crystal; Inset: Semi-log scale analysis of Femi-level versus VBM position (d) The energy level diagram of $Cs_2AgBiBr_6$ single crystal and different electrodes (Au, Ag and Al).

We propose that the superior Ohmic contact of Ag and $Cs_2AgBiBr_6$ single crystal versus Al and Au is due to the strong interaction of Ag and $Cs_2AgBiBr_6$. There are two possible explanations about Ohimic contact using Ag electrodes: 1) In Fig. 1c, it is observed that every $[AgBr_6]^{5-}/[BiBr_6]^{3-}$ octahedron in the crystal structure of $Cs_2AgBiBr_6$ is surrounded by six $[BiBr_6]^{3-}/[AgBr_6]^{5-}$ octahedra, because there exist evident differences between the charges of Ag^+ and Bi^{3+} cations to form the different coordination environment in the crystal structure. Thus, $Cs_2AgBiBr_6$ exhibits a disordered crystal structure at room temperature, which is consistent with the previous reports.[22, 39] Based on the lattice-matching theory and size effect about ionic radius,[40] Ag atoms can easily permeate into the $Cs_2AgBiBr_6$ single crystals and balance the charge leading to the better Ohmic contact of Ag electrode than Au and Al electrodes. 2) $Cs_2AgBiBr_6$ exhibited the *n*-type semiconductor properties. According to the energy band bending theory, when the metal work function is smaller than the semiconductors, as shown in Fig. S8, there exists no Schottky barrier and the metal-semiconductor contact using Ag electrodes is Ohmic, and vice versa based on the devices using Au electrodes in Fig. S8.[41-42] Therefore, $Cs_2AgBiBr_6$ single crystals exhibit the superior Ohmic contact, which can effectively reduce the contact barrier, which helps promote charge carrier transport. It is demonstrated that the electron barrier transports from Ag electrodes to $Cs_2AgBiBr_6$ perovskite single crystals in the dark to illustrate that the WF of Ag

electrodes minus the $Cs_2AgBiBr_6$ electron affinity, which helps form the good Ohmic contact. The response time is a key parameter to evaluate the performance of photodetectors. The rise time (t_{rise}) and fall time (t_{fall}) are defined as the increase from 10% to 90% of maximum value and decrease from 90% to 10% of maximum value, respectively in Fig. S9. The corresponding rise/fall times of $Cs_2AgBiBr_6$ single crystal photodetector in air and under vacuum are 159/85 ms and 75/38 ms, respectively, which is better than the $Cs_2AgBiBr_6$ thin film as seen in Table S3. Besides, based on the above energy level and experimental result analysis about electrodes, we observe the dark current decrease of $Cs_2AgBiBr_6$ single crystal devices based on different wavelengths from Au, Ag and Al in this order in air and vacuum atmosphere at 293 K in Fig. 3 and Fig. S7. $Cs_2AgBiBr_6$ single crystal devices using Au and Al exhibit the obvious hysteresis with photocurrent increase like memristor behaviors.[43] The photocurrent reduced quickly in vacuum than in air. The possible reason for the photocurrent to reduced more quickly in vacuum than in air is that oxygen and H_2O in air affect the surface of the double perovskite device and have an impact on the photocurrent, compared with the vacuum case.[47, 48] We also measured the stability of $Cs_2AgBiBr_6$ single crystal photodetectors in air and vacuum atmosphere when exposed to 400 nm condition. $Cs_2AgBiBr_6$ single crystal photodetectors exhibited the relatively good stability in Fig. S10. These intriguing results can provide guidance for obtaining high performance lead-free perovskite $Cs_2AgBiBr_6$ single crystal optoelectronic devices.

Finally, we investigate the $Cs_2AgBiBr_6$ single crystal photodetector performance at low temperature. Based on the previous report about the phase transition of $Cs_2AgBiBr_6$ materials,[12] we found that our $Cs_2AgBiBr_6$ single crystals also undergo phase transition. As shown in Fig. S2, $Cs_2AgBiBr_6$ single crystals exhibited two different crystal structures above and below the phase transition point (293 K and 100 K), which was consistent with the results previously reported by Radaelli et al. [12] To investigate the Ohmic contact behaviors at the $Cs_2AgBiBr_6$/Ag interfaces below and above the phase transition point, we carried out the $Cs_2AgBiBr_6$ single crystal photodetectors measurement using Ag electrodes in vacuum atmosphere at 293 K and 100 K. We carried out the photodetector measurements in vacuum atmosphere at 100 K at different applied voltages with a solar simulator (power intensity of 66.3 mW/cm^2) and at different wavelengths, as shown in Fig. 4 and Fig. S11. It was found that $Cs_2AgBiBr_6$ single crystals did not exhibit Ohmic contact behaviors at the low temperature of 100 K, as shown in Fig. 4 and Fig. S11. This observation is different from the above studies at room temperature in vacuum in Fig. 3. In particular, with the light turned on and off for several cycles using the different wavelengths, the dark current of $Cs_2AgBiBr_6$ single crystal was shifted. The formation of poor Ohmic contact for $Cs_2AgBiBr_6$/Ag photodetectors at low temperature is possibly caused by the changes of crystal structure arrangements induced by the temperature-dependent phase transition.[44] Therefore, high-performance optoelectronic devices with good Ohmic contact can be achieved based on the proper temperature and suitable electrodes about perovskite single crystal materials.

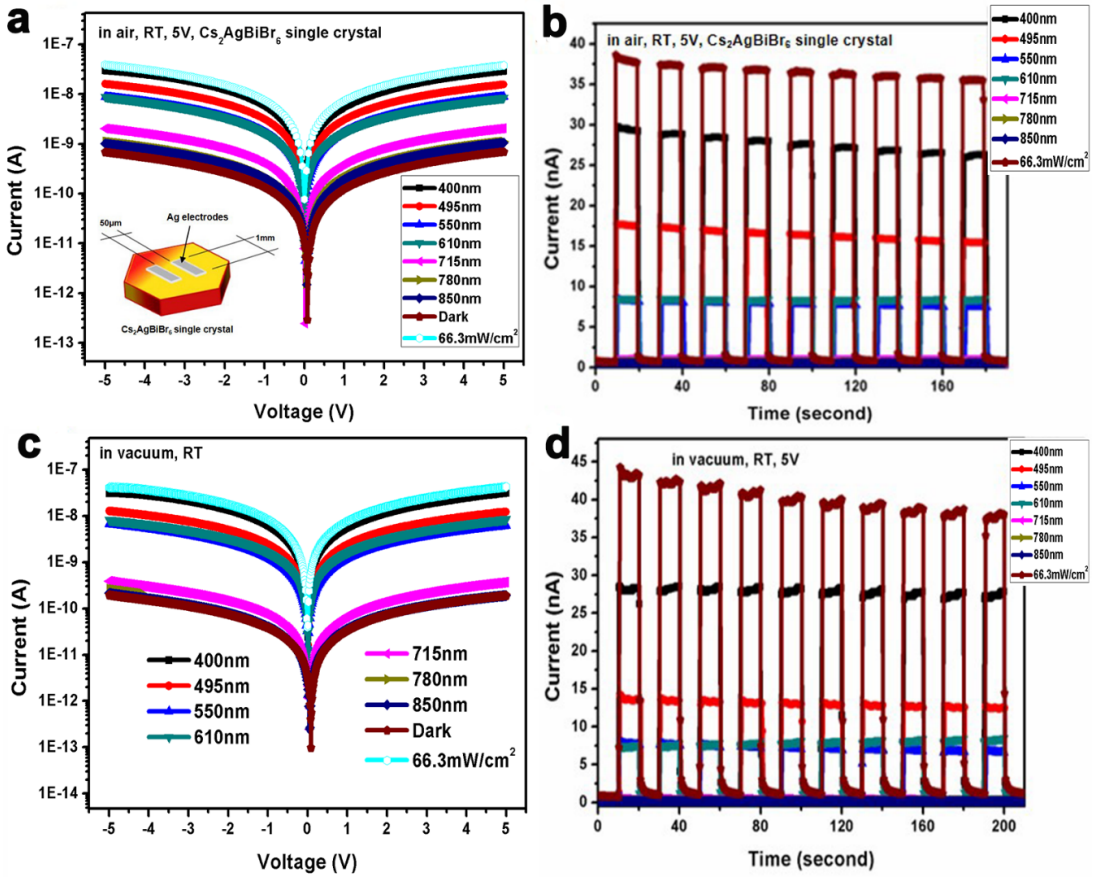

Fig. 3 (**a-d**) Photodetector data (I-V and I-time curves) of $Cs_2AgBiBr_6$ single crystals based on Ag electrodes at bias voltage (5V) when measured (a-b) in air with a relative humidity of 20% and (c-d) in vacuum (P = 3 × 10^{-7} Torr)

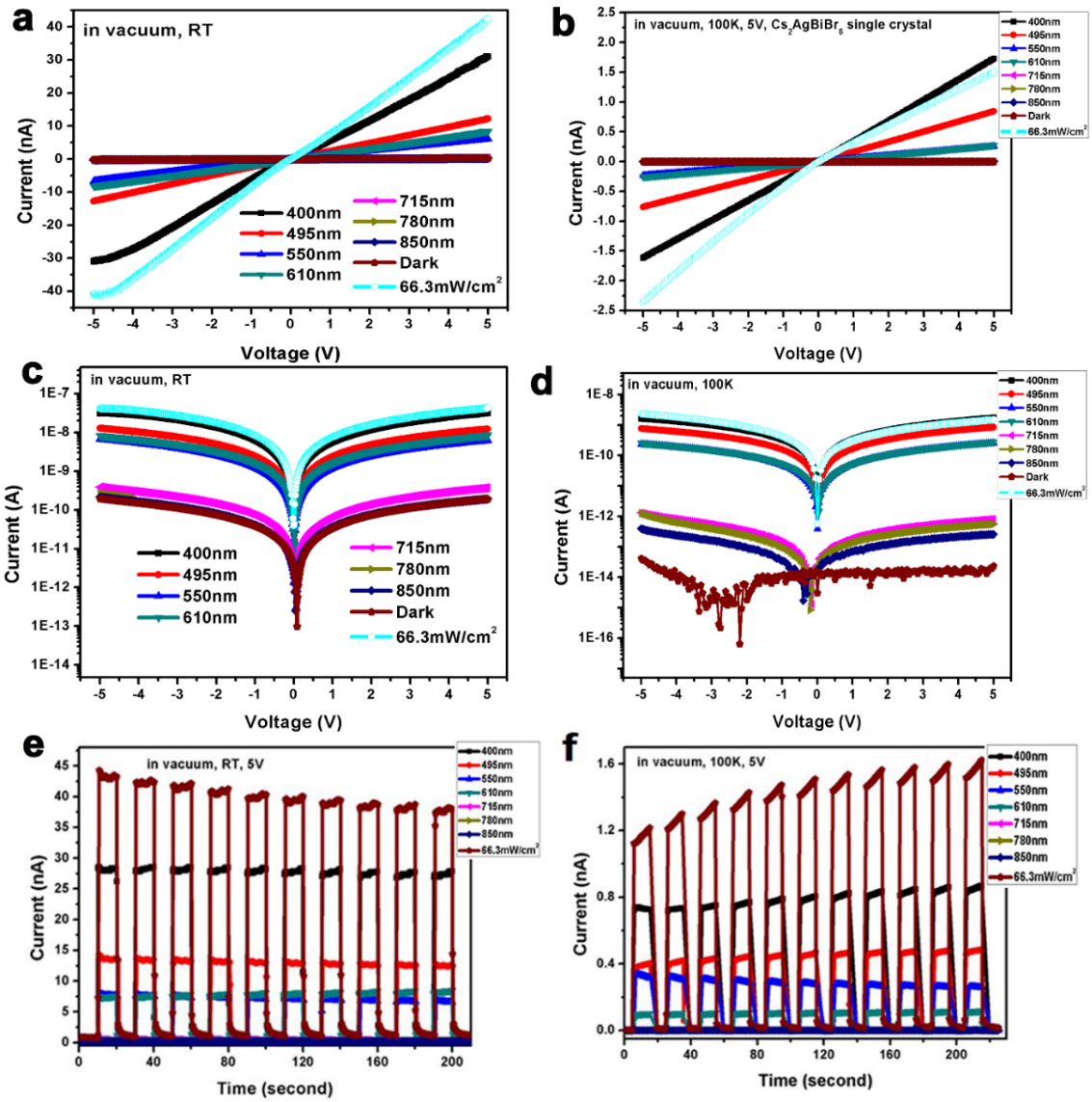

Fig. 4 (**a, c, e**) Photodetector data (I-V and I-time curves) of $Cs_2AgBiBr_6$ single crystal based on Ag electrodes under different wavelengths at room temperature; (**b, d, f**) Photodetector data (I-V and I-time curves) of $Cs_2AgBiBr_6$ single crystal based on Ag electrodes under different wavelengths at 100 K. All the measurements are performed under vacuum conditions (P = 3 ×10^{-7} Torr).

Conclusions

In summary, we obtained large-size $Cs_2AgBiBr_6$ double perovskite single crystal by means of the addition of MABr as flux. The optical band gap, XPS and UPS measurements were performed on $Cs_2AgBiBr_6$ single crystals. Photodetectors based on $Cs_2AgBiBr_6$ single crystals with different electrodes Au, Ag, and Al under a light source with different wavelength filters were studied. In addition, the influences of environment (air and vacuum atmospheres) as well as temperature (293 K and 100 K). It is concluded that photodetectors based on $Cs_2AgBiBr_6$ single crystal exhibit excellent photo-response by achieving Ohmic contact with Ag electrodes. In addition, photodetectors based on $Cs_2AgBiBr_6$ single crystal with Ag electrodes at room and low temperature conditions under which phase transition occurred were also systematically investigated. We believe that the present work not only provides an effective way to understand the intrinsic properties of $Cs_2AgBiBr_6$ single crystal, but also pave the way for high-performance $Cs_2AgBiBr_6$ single crystal photodetectors.

Experimental

Reagents

All starting reagents included Cs_2CO_3 (97%, Wako), Ag_2CO_3 (99%, Sigma-Aldrich), $(BiO)_2CO_3$ (80-82.5% Bi basis, Sigma-Aldrich), Methylammonium Bromide (99%, Dyesol), HBr (48%, Sigma-Aldrich) and H_3PO_2 (50 wt. % in H_2O, Sigma-Aldrich) solutions were used without further purifications.

Synthesis and crystal growth

The precursor synthesis of Cs_2CO_3, Ag_2CO_3 and $(BiO)_2CO_3$ in HBr and H_3PO_2 mixed solution was performed according to the chemical stoichiometric ratios. The Cs_2CO_3 (6.5100 g, 0.020 mol), Ag_2CO_3 (2.7500 g, 0.010 mol), $(BiO)_2CO_3$(5.0997 g, 0.010 mol) and MABr (2.2400 g, 0.02mol) were dissolved in 200 ml HI and 20ml H_3PO_2

mixed solution at 80°C under constant stirring, forming a yellow transparent solution after three days. Solutions were saturated at 75 °C. Large size $Cs_2AgBiBr_6$ single crystals were grown by temperature-lowering method by top-seeded solution growth (TSSG) method in an ambient atmosphere for about two weeks, as shown in **Fig. 1a**.

XPS and UPS measurements of $Cs_2AgBiBr_6$ single crystals

$Cs_2AgBiBr_6$ single crystals were cleaved and then fixed to the sample holders, as shown in **Fig. 2a**. The UPS and XPS spectra were measured on the X-ray photoelectron spectrometer (XPS-AXIS Ultra HAS, Kratos) equipped with monochromatic Al-Kα (1486.6 eV) and nonmonochromatic He-I (21.22 eV) sources, respectively. All the measurements were carried out in vacuum atmosphere ($<10^{-5}$ Pa).

Photodetector device fabrications and measurements

The single crystal photodetectors with planar-structure were fabricated by depositing ≈ 80 nm different electrodes (Au, Ag and Au) with a shadow mask (with a spacing of 1 mm × 50 μm) via thermal evaporation method on the surfaces of polished $Cs_2AgBiBr_6$ single crystals. The photo-response characteristics for the $Cs_2AgBiBr_6$ photodetectors were collected by a *Keithly 4200* semiconducting equipment. Monochromatic light was obtained by filtering the white light from a solar simulator with optical filters (400, 495, 550, 610, 715, 780 and 850 nm). The intensities of irradiated light are calibrated by optical power meter.

[CCDC **1919712-1919714** contain the supplementary crystallographic data for this paper. These data can be obtained free of charge from The Cambridge Crystallographic Data Centre via www.ccdc.cam.ac.uk/data_request/cif.

Conflicts of interest

There are no conflicts to declare.

Acknowledgements

This work is supported by funding from the Energy Materials and Surface Sciences Unit of the Okinawa Institute of Science and Technology Graduate University, the OIST Proof of Concept (POC) Program, and the OIST R&D Cluster Research Program. All the authors thank Dr. Maowei Jiang for his help in the Al evaporation fabrications of $Cs_2AgBiBr_6$ single crystals.

Notes and references

1 (a) L. K. Ono, Y. B. Qi, S. -F. Liu, *Joule* 2018, **2**, 1961. (b) S. Wang, Y. Jiang, E. J. Juarez-Perez, L. K. Ono, Y. B. Qi, *Nat. Energy* 2016, **2**, 16195.

2 (a) A. Kojima, K. Teshima, Y. Shirai, T. Miyasaka, *J. Am. Chem. Soc.* 2009, **131**, 6050. (b) Z. Chen, Q. Dong, Y. Liu, C. Bao, Y. Fang, Y. Lin, S. Tang, Q. Wang, X. Xiao, Y. Bai, Y. Deng, J. Huang, *Nat. Commun*. 2017, **8**, 1890.

3 National Renewable Energy Labs (NREL) Efficiency Chart, https://www.nrel.gov/pv/cell-efficiency.html

4 C. N. Savory, A. Walsh, D. O. Scanlon, *ACS Energy Lett.* 2016, **1**, 949.

5 E.T. McClure, M. R. Ball, W. Windl, P. M. Woodward, *Chem. Mater.* 2016, **28**, 1348.

6 F. Wei, Z. Deng, S. Sun, F. Zhang, D. M. Evans,G. Kieslich, S. Tominaka, M. A. Carpenter, J. Zhang, P. D. Bristowe, A. K. Cheetham, *Chem. Mater.* 2017, **29**, 1089.

7 F. Igbari, Z. -K. Wang, and L. -S. Liao, *Adv. Energy Mater.* 2019, **9**, 1803150.

8 G. Volonakis, M. R. Filip, A. A. Haghighirad, N. Sakai, B. Wenger, H. J. Snaith, F. Giustino, *J. Phys. Chem. Lett.*2016, **7**, 1254.

9 M. R. Filip, S. Hillman, A. A. Haghighirad, H. J. Snaith. F. Giustino, *J. Phys. Chem. Lett.*2016, **7**, 2579.

10 M. R. Filip, X. Liu, A. Miglio, G. Hautier, F. Giustino, *J. Phys. Chem. C* 2018, **122**, 158.

11 J. Yang, P. Zhang, and S. -H. Wei, *J. Phys. Chem. Lett.* 2018, **9**, 31.

12 L. Schade, A. D. Wright, R. D. Johnson, M. Dollmann, B. Wenger, P. K. Nayak, D. Prabhakaran, L. M. Herz, R. Nicholas, H. J. Snaith, P. G. Radaelli, *ACS Energy Lett.* 2019, **4**, 299.

13 (a)Z. Weng, J. Qin, A. A. Umar, J. Wang, X. Zhang, H. Wang, X. Cui, X. Li, L. Zheng, Y. Zhan, *Adv. Funct. Mater.* 2019, **29**, 1902234. (b) L. Yin, H. Wu, W. Pan, B. Yang, P. Li, J. Lu, G. Niu, J. Tang, *Adv. Opt. Mater*., 2019, **7**, 1900491.

14 E. Greul, M. L. Petrus, A. Binek, P. Docampo, T. Bein, *J. Mater. Chem. A* 2017, **5**, 19972.

15 C. Wu, Q. Zhang, Y. Liu, W. Luo, X. Guo, Z. Huang, H. Ting, W. Sun, X. Zhong, S. Wei, S. Wang, Z. Chen, L. Xiao, *Adv. Sci.* 2018, **5**, 1700759.

16 B. Yang, W. Pan, H. Wu, G. Niu, J. -H. Yuan, K. -H. Xue, L. Yin, X. Du, X. -S. Miao, X. Yang, Q. Xie, J. Tang, *Nat. Comm.* 2019,**10**, 1989.

17 Z. Chen, B. T. Abdullah, Y. Alsalloum, C. Yang, X. Zheng, I. Gereige, A. AlSaggaf, O. F. Mohammed, O. M. Bakr, *ACS Energy Lett.* 2019, **4**, 1258.

18 A. H. Slavney, T. Hu, A. M. Lindenberg, H. I. Karunadasa, *J. Am. Chem. Soc*. 2016, **138**, 2138.

19 W. Pan, H. Wu, J. Luo, Z. Deng, C. Ge, C. Chen, X. Jiang, W. -J. Yin, G. Niu, L. Zhu, L. Yin, Y. Zhou, Q. Xie, X. Ke, M. Sui, J. Tang, *Nat. Photon.* 2017, **11**, 726.

20 J. A. Steele, W. Pan, C. Martin, M. Keshavarz, E. Debroye, H. Yuan, S. Banerjee, E. Fron, D. Jonckheere, C. W. Kim, W. Baekelant, G. Niu, J. Tang, J. Vanacken, M. V. Auweraer, J. Hofkens, M. B. J. Roeffaers, *Adv. Mater.*2018, **30**, 1804450.

21 (a) W. Ning, X. -G. Zhao, J. Klarbring, S. Bai, F. Ji, F. Wang, S. I. Simak, Y. Tao, X. Ren, L. Zhang, W. Huang, I. A. Abrikosov, F. Gao, *Adv. Funct. Mater.*2019, **29**, 1807375. (b) J. Yang, C. Bao, W. Ning, B. Wu, F. Ji, Z. Yan, Y. Tao, J. -M. Liu, T. C. Sum, S. Bai, J. Wang, W. Huang, W. Zhang, F. Gao, *Adv. Optical Mater.* 2019, **7**, 1801732.

22 W. Yuan, G. Niu, Y. Xian, H. Wu, H. Wang, H. Yin, P. Liu, W. Li, J. Fan, *Adv. Funct. Mater.*2019, **29**, 1900234.

23 Z. Zhang, G. Yang, C. Zhou, C. -C. Chung and I. Hany, *RSC Adv.* 2019, **9**, 23459.

24 (a) Y. Dang, Y. Liu, Y. Sun, D. Yuan, X. Liu, W. Lu, G. Liu, H. Xia, X. Tao, *CrystEngComm* 2015, **17**, 665. (b) Y. Dang, C. Zhong, G. Zhang, D. Ju, L. Wang, S. Xia, H. Xia, X. Tao, *Chem. Mater.*2016, **28**, 6968.

25 Y. Dang, Y. Zhou, X. Liu, D. Ju, S. Xia, H. Xia, X. Tao, *Angew. Chem. Int. Ed.* 2016, **55**, 3447.

26 Y. Dang, D. Ju, L. Wang, X. Tao, *CrystEngComm* 2016, **18**, 4476.

27 Y. Dang, J. Wei, X. Liu, X. Wang, K. Xu, M. Lei, W. Hu, X. Tao, *Sustainable Energy Fuels*, 2018, **2**, 2237-2243

28 A. Bravais, Etudes cristal-géographiques; Academie des Sciences: Paris, 1913.

29 (a)J. Xiu, Y. Shao, L. Chen, Y. Feng, J. Dai, X. Zhang, Y. Lin, Y. Zhu, Z. Wu, Y. Zheng, H. Pan, C. Liu, X. Shi, X. Cheng, Z. He, *Materials Today Energy* 2019,**12**, 186.(b) T. Li, J. Wang, Z. Gao, P. Lv, Y. Yang, J. Wu, J. Hong, X. Wang, and Y. Zhou, *Appl. Phys. Lett.* 2019, **115**, 131103.

30 Z. Xiao, W. Meng, J. Wang, Y. Yan, *ChemSusChem* 2016, **9**, 2628.

31 W. Song, K. Leung, Q. Shao, K. J. Gaskell, and J. E. Reutt-Robey, *J. Phys. Chem. C* 2016, **120**, 22979-22988.

32 C. Wang, B. R. Ecker, H. Wei, J. Huang, J. Meng, Y. Gao, *Phys. Chem. Chem. Phys.*2017, **19**, 5361.
33 C. Li, J. Wei, M. Sato, H. Koike, Z. Xie, Y. Li, K. Kanai, S. Kera, N. Yeno, J. Tang, *ACS Appl. Mater. Interfaces* 2016, **8**, 11526.
34 J. Endres, D.A. Egger, M. Kulbak, R.A. Kerner, L. Zhao, S.H. Silver, G. Hodes, B.P. Rand, D. Cahen, L. Kronik, A. Kahn, *J. Phys. Chem. Lett.* 2016, **7**, 2722.
35 F. Zu, P. Amsalem, D.A. Egger, R. Wang, C.M. Wolff, H. Fang, M.A. Loi, D. Neher, L. Kronik, S. Duhm, N. Koch, *J. Phys. Chem. Lett.* 2019, **10**, 601.
36 (a) S. Wang, T. Sakurai, W. Wen, Y. B. Qi, *Adv. Mater. Interfaces* 2018, **5**, 1800260. (b) D. Meggiolaro, E. Mosconi, and F. De Angelis, *ACS Energy Le*t.2019, **4**, 779.
37 (a) R. H. Bube, *J. Appl. Phys.* 1962, **33**, 1733. (b) Y. Liu, J. Sun, Z. Yang, D. Yang, X. Ren, H. Xu, Z. Yang, S.-F. Liu, *Adv. Opt.l Mater*. 2016, **4**, 1829. (c) D. Shi, V. Adinol, R. Comin, M. Yuan, E. Alarousu, A. Buin, Y. Chen, S. Hoogland, A. Rothenberger, K. Katsiev, Y. Losovyj, X. Zhang, P. A. Dowben, O. F. Mohammed,E. H. Sargent, O. M. Bakr, *Science,* 2015, **347**, 519. (d) Q. Dong, Y. Fang, Y. Shao, P. Mulligan, J. Qiu, L. Cao, J. Huang, *Science*, 2015, **347**, 967.
38 M. A. Najeeb, Z. Ahmad, R. A. Shakoor A. Alashraf, J. Bhadra, N. J. Al-Thani, S. A. Al-Muhtaseb, A. M. A. Mohamed, *Opt. Mater.* 2017, **73**, 50.
39 P. Woodward, R. Hoffmann, A. Sleight, *J. Mater. Res*. 1994, **9**, 2118.
40 (a) A. Zur and T. C. McGill, *J. Appl. Phys.* 1984, **55**, 378. (b) X. Zhao, L. Li, M. Zhao, *J. Phys. Condens. Mat.* 2014, **26**, 095002.
41 Z. Zhang, J. T. Yates, Jr. *Chem. Rev.* 2012, **112**, 5520.
42 E. Shi, Y. Gao, B. P. Finkenauer, Akriti, A. H. Coffey, L. Dou, *Chem. Soc. Rev.* 2018, **47**, 6046.
43 W. Xu, H. Cho, Y. H. Kim, Y. T. Kim, C. Wolf, C. G. Park, T. W. Lee, *Adv. Mater.* 2016, **28**, 5916.
44 B. J. Foley, D. L. Marlowe, K. Sun, W. A. Saidi, L. Scudiero, M. C. Gupta J. J. Choi, *Appl. Phys. Lett.* 2015, **106**, 243904.
45 (a)E. Greul, M. L. Petrus, A. Binek, P. Docampo and T. Bein, *J. Mater. Chem. A*, 2017,**5**, 19972. (b) S. J. Zelewski, J. M. Urban, A. Surrente, D. K. Maude, A. Kuc,L. Schade, R. D. Johnson, M. Dollmann, P. K. Nayak, H. J. Snaith, P. Radaelli, R. Kudrawiec, R. J. Nicholas, P. Plochocka and M. Baranowski, *J. Mater. Chem. C,* 2019,**7**, 8350.
46 (a) G. Tong, X. Geng, Y. Yu, L. Yu, J. Xua, Y. Jiang, Y. Sheng, Y. Shi and K. Chen, RSC Adv., 2017, **7**, 18224; (b) L. Dou, Y. M. Yang, J. You, Z. Hong. W. H. Chang, G. Li, and Y. Yang, *Nat. Commun.*, 2014, **5**, 5404; (c) S. Gu,K. Ding, J. Pan, Z. Shao, J. Mao, X. Zhang and J. Jie, *J. Mater. Chem. A*, 2017,**5**, 11171. (d) J. Miao, F. Zhang, *Laser Photonics Rev*. 2019, **13**, 1800204
47 H.-H. Fang, S. Adjokatse, H. Wei, J. Yang, G. R. Blake, J. Huang, J. Even, M. A. Loi, *Sci. Adv*. 2016, **2**, e1600534.
48 R. Brenes, C. Eames, V. Bulović, M. S. Islam, S. D. Stranks, *Adv. Mater*. 2018, **30**, 1706208.

